# Diffusion-weighted Endorectal MR Imaging at 3 T for Prostate Cancer: Tumor Detection and Assessment of Aggressiveness[1]

Hebert Alberto Vargas, MD
Oguz Akin, MD
Tobias Franiel, MD
Yousef Mazaheri, PhD
Junting Zheng, MS
Chaya Moskowitz, PhD
Kazuma Udo, MD
James Eastham, MD
Hedvig Hricak, MD, PhD, Dr(hc)

**Purpose:** To assess the incremental value of diffusion-weighted (DW) magnetic resonance (MR) imaging over T2-weighted MR imaging at 3 T for prostate cancer detection and to investigate the use of the apparent diffusion coefficient (ADC) to characterize tumor aggressiveness, with whole-mount step-section pathologic analysis as the reference standard.

**Materials and Methods:** The Internal Review Board approved this HIPAA-compliant retrospective study and waived informed consent. Fifty-one patients with prostate cancer (median age, 58 years; range, 46–74 years) underwent T2-weighted MR imaging and DW MR imaging ($b$ values: 0 and 700 sec/mm$^2$ [$n$ = 20] or 0 and 1000 sec/mm$^2$ [$n$ = 31]) followed by prostatectomy. The prostate was divided into 12 regions; two readers provided a score for each region according to their level of suspicion for the presence of cancer on a five-point scale, first using T2-weighted MR imaging alone and then using T2-weighted MR imaging and the ADC map in conjunction. Areas under the receiver operating characteristic curve (AUCs) were estimated to evaluate performance. Generalized estimating equations were used to test the ADC difference between benign and malignant prostate regions and the association between ADCs and tumor Gleason scores.

**Results:** For tumor detection, the AUCs for readers 1 and 2 were 0.79 and 0.76, respectively, for T2-weighted MR imaging and 0.79 and 0.78, respectively, for T2-weighted MR imaging plus the ADC map. Mean ADCs for both cancerous and healthy prostatic regions were lower when DW MR imaging was performed with a $b$ value of 1000 sec/mm$^2$ rather than 700 sec/mm$^2$. Regardless of the $b$ value used, there was a significant difference in the mean ADC between malignant and benign prostate regions. A lower mean ADC was significantly associated with a higher tumor Gleason score (mean ADCs of [1.21, 1.10, 0.87, and 0.69] $\times$ 10$^{-3}$ mm$^2$/sec were associated with Gleason score of 3 + 3, 3 + 4, 4 + 3, and 8 or higher, respectively; $P$ = .017).

**Conclusion:** Combined DW and T2-weighted MR imaging had similar performance to T2-weighted MR imaging alone for tumor detection; however, DW MR imaging provided additional quantitative information that significantly correlated with prostate cancer aggressiveness.



[1] From the Departments of Radiology (H.A.V., O.A., Y.M., H.H.), Medical Physics (Y.M.), Epidemiology and Biostatistics (J.Z., C.M.), Pathology (K.U.), Urology (J.E.), and Surgery (J.E.), Memorial Sloan-Kettering Cancer Center, 1275 York Ave, Room C-278, New York, NY 10065; and Department of Radiology, Charité, Universitätsmedizin Berlin, Berlin, Germany (T.F.). Received October 15, 2010; revision requested November 26; revision received December 22; accepted January 10, 2011; final version accepted January 18. T.F. supported by the German Research Foundation (grant DFG-FR 2891/1-1). **Address correspondence to** H.A.V. (e-mail: *vargasah@mskcc.org*).

The prostate is the most common noncutaneous site of cancer among men in the United States (1). Owing to the increasing awareness of its variable biologic aggressiveness, the biggest challenge in managing patients with newly diagnosed prostate cancer is shifting from tumor detection alone to identifying patients with aggressive disease who would benefit from more radical therapy, while sparing those with indolent cancers. There is an increasing need for translational research addressing this clinical challenge. Functional magnetic resonance (MR) imaging techniques are garnering substantial interest as possible means to stratify patients with prostate cancer by risk (2–7). These techniques, which include MR spectroscopic imaging, diffusion-weighted (DW) MR imaging, and dynamic contrast material–enhanced MR imaging, can provide qualitative and quantitative information regarding tumor biology.

In theory, combining multiple functional MR imaging techniques with standard anatomic imaging sequences could make MR imaging a much more powerful tool for noninvasively characterizing prostate cancer. However, practical methods to analyze, interpret, and integrate the large amount of data generated by such a multiparametric approach are still lacking. Of all the available functional MR imaging methods, DW MR imaging is the one most commonly integrated into clinical prostate MR imaging protocols because it possesses a number of advantages: Its acquisition time is short, it does not require the administration of contrast material, and generating qualitative and quantitative parametric image maps based on the apparent diffusion coefficient (ADC) is straightforward by using commercially available software.

Recent advances in MR imaging technology, such as 3-T magnets, multichannel coils, and parallel imaging, have allowed higher signal-to-noise ratios that enhance the quality of anatomic as well as functional MR imaging. Studies (8–11) have shown that adding DW MR imaging to conventional MR imaging at 3 T may improve the assessment of prostate cancer. While these preliminary reports are encouraging, DW MR imaging is still an evolving technique with several limitations to be overcome; these include intrinsic technical difficulties that result in image distortions and susceptibility artifacts and a lack of standardized acquisition and image analysis methods. More importantly, the diagnostic performance of DW MR imaging in characterizing prostate cancer needs to be further studied.

Thus, the purpose of our study was to assess the incremental value of DW MR imaging over T2-weighted MR imaging at 3 T for prostate cancer detection and to investigate the use of the ADC to characterize tumor aggressiveness, with whole-mount step-section pathologic specimens as the reference standard.

### Advance in Knowledge

- While T2-weighted MR imaging alone performed similarly to combined DW and T2-weighted MR imaging for tumor detection, the addition of DW MR imaging was useful for the assessment of prostate cancer aggressiveness, as indicated by a significant inverse correlation between apparent diffusion coefficients (ADCs) and Gleason scores ($P = .017$).

## Materials and Methods

The institutional review board approved our retrospective study and waived the informed consent requirement. Our study was compliant with the Health Insurance Portability and Accountability Act.

### Eligibility Criteria and Patient Characteristics

The inclusion criteria for our study were as follows: (i) endorectal MR imaging, including DW MR imaging, performed at 3 T for the assessment of prostate cancer between September 2008 and May 2009; (ii) radical prostatectomy performed at our institution within 6 months after the MR imaging; and (iii) whole-mount step-section pathologic tumor maps available. We excluded patients with (i) prior prostate cancer treatment, including surgery, focal therapy, hormones, or radiation, and (ii) MR imaging artifacts that made the examination nondiagnostic. Through computerized searches of our urology department database, we identified 288 patients who had undergone radical prostatectomy during the study period and had whole-mount step-section pathologic tumor maps available. Of these patients, 238 had undergone prostate MR imaging within the 6 months preceding the prostatectomy. For 175 of these patients, the MR imaging examination included DW MR imaging. In 55 of these patients, the examination was performed at 3 T. One of the 55 patients was excluded because he had received prior radiation therapy, and three were excluded because of marked distortion of DW MR imaging caused by motion or susceptibility artifacts. Thus, our study included a

### Implication for Patient Care

- The ADC derived from diffusion-weighted MR imaging allows the identification of patients with aggressive prostate cancer and may facilitate appropriate treatment selection.

**Published online before print**
10.1148/radiol.11102066

**Radiology 2011;** 259:775–784

**Abbreviations:**
ADC = apparent diffusion coefficient
AUC = area under receiver operating characteristic curve
CI = confidence interval
DW = diffusion weighted
ROI = region of interest

**Author contributions:**
Guarantors of integrity of entire study, H.A.V., O.A.; study concepts/study design or data acquisition or data analysis/interpretation, all authors; manuscript drafting or manuscript revision for important intellectual content, all authors; approval of final version of submitted manuscript, all authors; literature research, H.A.V., O.A., T.F., Y.M., K.U.; clinical studies, H.A.V., O.A., T.F., K.U.; experimental studies, Y.M., K.U.; statistical analysis, J.Z., C.M.; and manuscript editing, H.A.V., O.A., J.Z., C.M., K.U., J.E.

**Funding:**
This research was supported by the National Institutes of Health (grant R01 CA76423).

Potential conflicts of interest are listed at the end of this article.

total of 51 patients. A summary flowchart of patient selection is presented in Figure 1 and the patients' characteristics are presented in Table 1.

### MR Imaging Acquisition

MR imaging studies were performed by using a 3-T whole-body unit (Signa HDX; GE Medical Systems, Milwaukee, Wis). A body coil was used for excitation; a pelvic four-channel phased-array coil and a balloon-covered expandable endorectal coil (Medrad, Warrendale, Pa) filled with air were used for signal reception. The anatomic images were obtained by using transverse T1-weighted (repetition time msec/echo time msec, 600–750/10–14; section thickness, 5 mm; intersection gap, 1 mm; field of view, 28–36 cm; matrix, 256 × 192) and transverse, coronal, and sagittal T2-weighted fast spin-echo (3500/120; echo train length, 12–16; section thickness, 3 mm; no intersection gap; field of view, 14–16 cm; matrix, 256 × 192) sequences. DW MR imaging was obtained in the transverse plane with orientation and location identical to those prescribed for the transverse T2-weighted MR imaging by using a spin-echo echo-planar imaging sequence with ramp sampling by using a pair of rectangular gradient pulses along with three orthogonal axes (repetition time msec/effective echo time msec, 3500/63.5–108.4 [median 82 msec]; field of view, 14 cm; section thickness, 3 mm; no intersection gap; in-plane resolution, 1.9 × 1.9 mm; *b* values, 0 and 700 sec/mm$^2$ [$n$ = 20] or 0 and 1000 sec/mm$^2$ [$n$ = 31]). Parametric image maps based on ADCs were generated by using Advanced Workstation software (GE Medical Systems).

### MR Imaging Interpretation

Two radiologists retrospectively and independently interpreted the MR imaging studies, which were archived in a picture archiving and communication system (Centricity; GE Medical Systems). At the time of the study, reader 1 (H.A.V.) was a body imaging fellow with a special interest and 2 years experience in prostate MR imaging, and reader 2 (T.F.) was a radiologist with 4 years experience interpreting prostate MR imaging. The readers were aware that the patients had prostate cancer, but they were blinded to clinical, laboratory (including prostate-specific antigen values), biopsy results (including tumor locations and histologic findings), and the original MR imaging reports.

*Qualitative assessment.*—The readers evaluated twelve regions of the prostate by applying the sextant schema (right and left base, midgland, and apex) in both the peripheral and transition zones. For all regions, the readers independently assigned scores for the likelihood of cancer on a five-point index scale (1 = definitely absent, 2 = probably absent, 3 = indeterminate, 4 = probably present, 5 = definitely present). First they assigned scores based on the interpretation of T2-weighted images alone. Then, they evaluated each region by using a combination of T2-weighted images and the parametric ADC map derived from the DW MR images and assigned a new set of scores. For the purposes of image interpretation, tumor was defined as a focal or nodular area that displayed (i) focal low signal intensity on T2-weighted images and/or (ii) focal restricted diffusion on the ADC map (Fig 2).

*Quantitative assessment.*—The readers independently recorded the two-dimensional measurements of each lesion with a diameter of at least 4 mm that they identified on the T2-weighted images and/or ADC parametric maps. For the quantitative analysis of DW MR imaging parameters, one of the authors (H.A.V.) placed a region of interest (ROI) to cover each lesion detected by at least one reader. After all MR imaging readings were completed, by using the whole-mount step-section pathology maps as a guide, additional ROIs were placed in noncancerous regions in the peripheral and transition zones in each patient as well as to cover any cancer foci missed by the readers but identified on pathology maps. The ROIs were placed on the ADC map by using the freehand drawing tool on Advanced Workstation software to encompass as much of the inner aspect of the lesion as possible

**Figure 1**

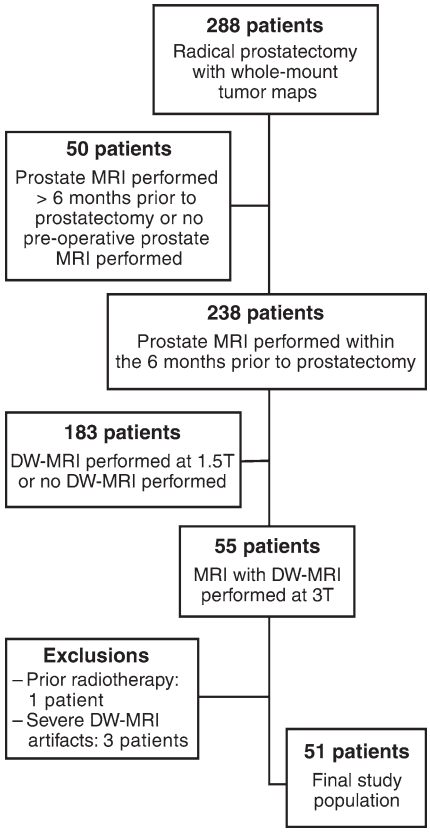


**Figure 1:** Flowchart summarizing patient selection. *DW-MRI* = DW MR imaging.

**Table 1**

**Patient Characteristics**

| Characteristic | Value |
|---|---|
| Age (y) | 58 (46–74)* |
| Initial prostate-specific antigen (ng/mL) | 5.3 (0.4–62.2)* |
| Time between MR imaging and prostatectomy (d) | 25 (1–181)* |
| Gleason score | |
| Biopsy | |
| 3 + 3 | 18 (35) |
| 3 + 4 | 19 (37) |
| 4 + 3 | 9 (18) |
| ≥4 + 4 | 5 (10) |
| Prostatectomy | |
| 3 + 3 | 10 (20) |
| 3 + 4 | 26 (51) |
| 4 + 3 | 13 (25) |
| ≥4 + 4 | 2 (4) |

Note.—Unless otherwise specified, data are number of patients, with percentage of 51 total patients in parentheses.

* Data are median, with range in parentheses.

without contacting the edges. There were between zero and four ROIs per patient with a mean area of 33 $mm^2$ (range, 8–159 $mm^2$). The mean ADC within each ROI was recorded. The ADC ratio was obtained by dividing the ADC of a cancer ROI by the ADC of an area of noncancerous tissue in the same prostate zone (ie, peripheral or transition) as the cancer focus.

### Histopathologic Analysis and Image Correlation

Prostatectomy specimens were sliced from apex to base at 3–4-mm intervals. The distal 5-mm portion of the apex was amputated and coned. The seminal vesicles were amputated and submitted separately. After paraffin embedding, microslices were placed on glass slides and stained with hematoxylin-eosin. Each lesion was measured in size and assigned a Gleason score by a pathology fellow (K.U.) with 3 years experience in genitourinary pathology, whose findings were verified by one of the staff genitourinary pathologists at our institution. The Gleason scores for the biopsy and prostatectomy specimens were recorded. MR imaging findings were correlated with the whole-mount prostatectomy findings approximately 4 weeks after the MR imaging readings were performed. This was done in consensus by three of the authors (K.U., H.A.V., and T.F.) in a single session, where the whole-mount pathology maps were evaluated in conjunction with the MR imaging to establish the location of tumors with respect to the prostatic urethra (anterior, posterior, right, and/or left) and other anatomic landmarks (eg, prostate zones, ejaculatory ducts, and verumontanum), subjectively allowing for distortions in the prostate size and shape caused in vivo by the presence of the endorectal coil and ex vivo by the preparation of the whole-mount pathology specimen (eg, tissue shrinkage during fixation).

### Statistical Analysis

The pathologic findings from prostate biopsy and radical prostatectomy (eg, Gleason scores, tumor sizes and locations) were summarized by using frequencies and percentages. Reader performance in qualitative interpretation of MR imaging studies was analyzed at the prostate region level. The sensitivity and specificity were estimated by treating those regions with a score of 3 or greater as positive for cancer. The corresponding 95% confidence intervals (CIs) for these estimated measures of accuracy were calculated by using variance estimates that take into account the correlated data owing to the multiple regions within a patient (12). Score statistics based on the generalized estimating equations method with an independent working correlation matrix were used to test the equality of the measurement of accuracy (13). Receiver operating characteristic curves and the areas under these curves (AUCs) were estimated nonparametrically for the ordinal score assessments. The AUCs for T2-weighted MR imaging alone versus the combination of T2-weighted and DW MR imaging were compared by using a nonparametric method proposed by Obuchowski (14). Post hoc power calculation for measures of accuracy was performed by using published sample size equations (15). The estimation of the power was based on a two-sided test with 5% type I error rate under the following assumptions: the sensitivity was 0.65 (sensitivity of T2-weighted MR imaging alone) under the null hypothesis and the specificity was 0.88 (specificity of T2-weighted MR imaging alone) under the null hypothesis. Interreader agreement was evaluated by using the weighted κ statistic with quadratic weights (16), which was interpreted based on the table provided by Landis and Koch (17).

For the quantitative analysis of DW MR imaging, score statistics from generalized estimating equations with an independent working correlation matrix accounting for the correlated data were used to test the ADC mean difference between the ROIs in each region as categorized by MR imaging and whole-mount step-section pathology correlation. The mean ADCs, ADC ratios, standard errors, and corresponding *P* values were calculated for the score statistics. The same methods were used to perform a subgroup analysis for patients in whom the DW MR imaging was acquired with *b* values of 0 and 700 $sec/mm^2$ versus those in whom the *b* values used were 0 and 1000 $sec/mm^2$. To assess the degree of overlap between the distribution of ADCs in prostate cancer lesions and those in healthy prostate tissue at the different *b* values, taking into account the variability in the data, we fit a regression model that included an interaction term between tissue type (cancer lesions and healthy prostate) and subgroup ($b$ = 700 $sec/mm^2$ and $b$ = 1000 $sec/mm^2$).

**Figure 2**

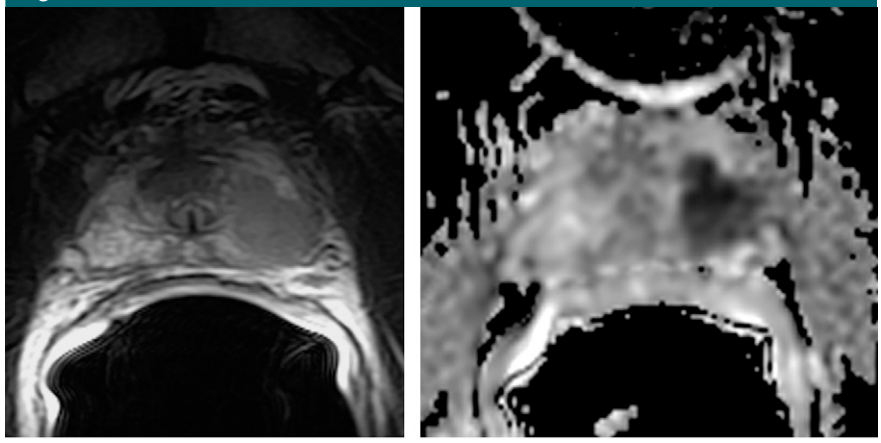

a. b.

**Figure 2:** Gleason score 7 (4 + 3) tumor of the left prostatic apex in a 65-year-old patient is seen as **(a)** a homogeneous focus of low signal intensity on a transverse T2-weighted MR image (3516/122) and **(b)** a focus of restricted diffusion on the ADC map (3500/76.3; *b* value, 700 $sec/mm^2$).

**Table 2**

**Qualitative Assessment of Diagnostic Performance**

| Statistic | Reader 1 | | | Reader 2 | | |
|---|---|---|---|---|---|---|
| | T2-weighted MR Imaging | T2-weighted and DW MR Imaging | *P* Value | T2-weighted MR Imaging | T2-weighted and DW MR Imaging | *P* Value |
| Sensitivity | 0.65 (0.56, 0.74) | 0.61 (0.52, 0.71) | .27 | 0.61 (0.51, 0.70) | 0.62 (0.53, 0.72) | .67 |
| Specificity | 0.88 (0.84, 0.93) | 0.94 (0.91, 0.97) | .01 | 0.85 (0.80, 0.90) | 0.86 (0.82, 0.90) | >.99 |
| Positive predictive value | 0.79 (0.73, 0.85) | 0.87 (0.82, 0.93) | .02 | 0.73 (0.66, 0.81) | 0.75 (0.68, 0.82) | .12 |
| Negative predictive value | 0.79 (0.72, 0.86) | 0.78 (0.72, 0.85) | .67 | 0.76 (0.69, 0.83) | 0.77 (0.70, 0.84) | .52 |

Note.—Data in parentheses are 95% CIs.

**Figure 3**

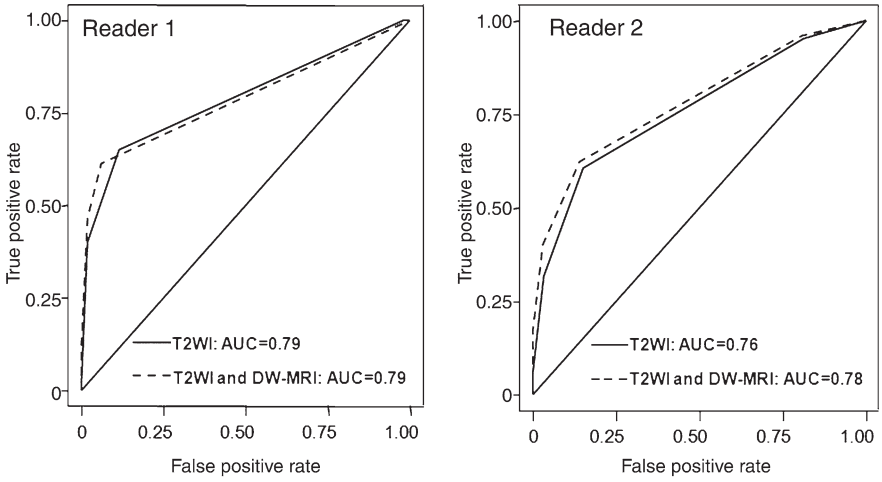


**Figure 3:** Receiver operating characteristic curves and AUCs for readers **(a)** 1 and **(b)** 2 for detection and localization of prostate cancer by using T2-weighted MR imaging *(T2WI)* with or without DW MR imaging *(DW-MRI)*.

The associations between the mean ADC, ADC ratio, and tumor Gleason score were assessed separately by using the generalized estimating equations method. A *P* value of less than .05 was considered to indicate a significant difference. All statistical analyses were performed with SAS 9.2 software (SAS Institute, Cary, NC).

## Results

### Histopathologic Results

At histopathologic analysis, a total of 89 cancer foci were found in the prostatectomy specimens of the 51 patients (peripheral zone, $n = 77$; transition zone, $n = 8$; both peripheral and transition zones, $n = 4$). The largest transverse dimension of the cancer foci at histopathologic analysis ranged from 3 to 35 mm, with a median of 11 mm. Gleason scores for biopsy versus prostatectomy specimens (Table 1) differed in 22 patients (43%). In 14 patients (27%), the surgicopathologic Gleason score was higher and in eight (16%) it was lower than the biopsy Gleason score. Among the 89 cancer foci found in the prostatectomy specimens, 32 were Gleason 3 + 3, 38 were Gleason 3 + 4, 15 were Gleason 4 + 3, and four were Gleason 4 + 4 or higher.

### MR Imaging Results

*Qualitative assessment.*—For prostate cancer detection at the region level, the AUCs for reader 1 were 0.79 (95% CI: 0.73, 0.85) with T2-weighted MR imaging alone and remained 0.79 (95% CI: 0.72, 0.85) with the combination of T2-weighted and DW MR imaging ($P = .099$), while the AUCs for reader 2 were 0.76 (95% CI: 0.70, 0.82) with T2-weighted MR imaging alone and improved to 0.78 (95% CI: 0.72, 0.84) with the addition of DW MR imaging ($P < .001$) (Fig 3). The latter *P* value, although significant, was considered clinically unimportant given the considerable overlap in 95% CIs and the small difference in AUC of 0.02 (reflecting an improvement of only about 2.6%). The small *P* value may be explained by the relatively large number of observations derived from region analysis (12 regions per patient in 51 patients = 612 regions) (18).

For reader 1, specificity and positive predictive value for tumor detection increased significantly from 0.88 to 0.94 ($P = .01$) and from 0.79 to 0.87 ($P = .02$), respectively, with the addition of DW MR imaging to T2-weighted MR imaging. However, no significant difference in sensitivity or negative predictive value was observed. For reader 2, the addition of DW MR imaging did not produce any significant difference in sensitivity, specificity, or positive or negative predictive value for the detection of prostate cancer foci (Table 2). Post hoc power calculation resulted in approximately 84% power to detect a specificity difference of 0.10 between T2-weighted MR imaging alone and T2-weighted MR imaging in combination with DW MR imaging and 45% power to detect a sensitivity difference of 0.10.

Interreader agreement for the detection of prostate cancer was moderate to substantial, with weighted κ statistics

**Figure 4**

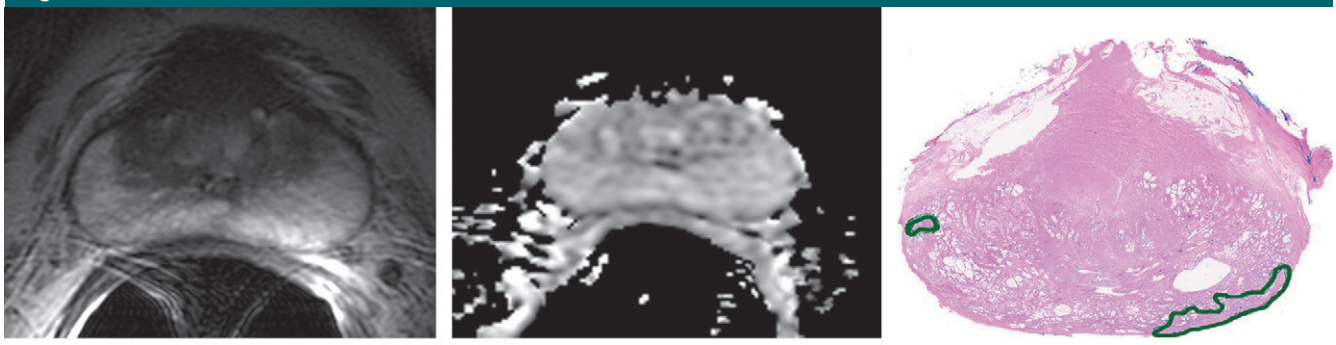

a. b. c.

**Figure 4:** Images from a 67-year-old patient with prostate cancer. No definite abnormality was seen on either the **(a)** T2-weighted MR image (3500/118) or **(b)** ADC map (3500/87.5; $b = 700$ sec/mm$^2$). **(c)** A representative image from step-section pathologic analysis shows tumor foci (outlined in green, Gleason 3 + 3) in right and left peripheral zones. (Hematoxylin-eosin stain; original magnification, ×1.05.)

of 0.60 for T2-weighted MR imaging alone and 0.64 for the combination of T2-weighted MR imaging and DW MR imaging.

*Lesion detection.*—Reader 1 correctly identified 65 (73%) of the 89 cancer foci, including 20 (63%) of 32 Gleason 3 + 3 lesions, 30 (79%) of 38 Gleason 3 + 4 lesions, 11 (73%) of 15 Gleason 4 + 3 lesions, and four (100%) of four Gleason 4 + 4 or higher lesions. Reader 2 correctly identified 61 (69%) of 89 lesions, including 17 (53%) of 32 Gleason 3 + 3 lesions, 27 (71%) of 38 Gleason 3 + 4 lesions, 13 (87%) of 15 Gleason 4 + 3 lesions, and four (100%) of four Gleason 4 + 4 or higher lesions. Of the 75 lesions that reader 1 identified as cancer by using T2-weighted and DW MR imaging, 10 (13%) were false-positive findings. Of the 74 lesions that reader 2 identified as cancer, 13 (18%) were false-positive findings.

Sixteen (18%) of the 89 cancer foci identified at step-section pathologic analysis were not visible at DW MR imaging (Fig 4). Of these 16 cancer foci, nine had a Gleason score of 3 + 3, and seven had a Gleason score of 3 + 4. The largest histopathologic transverse dimension of the tumor foci undetected on DW MR images ranged from 3 to 21 mm, with a median of 7 mm. Reader 1 detected one of these 16 cancer foci by using T2-weighted MR imaging alone, and reader 2 detected two.

*Correlation of ADC with step-section histopathologic findings.*—In the peripheral zone, the mean ADC of true-positive cancer lesions was significantly lower than that of healthy tissue for both readers (both $P < .001$). The mean ADC of the false-positive lesions did not differ significantly from the mean ADC of the true-positive lesions for either reader ($P = .95$ for reader 1, $P = .86$ for reader 2). Mean ADCs for both cancerous and healhty prostatic regions were lower when DW MR imaging was performed with a $b$ value of 1000 sec/mm$^2$ rather than 700 sec/mm$^2$. The mean ADCs for cancer lesions and healthy tissue were (1.33 ± 0.10 [standard error]) × $10^{-3}$ mm$^2$/sec and (2.14 ± 0.10) × $10^{-3}$ mm$^2$/sec for both readers in patients in whom $b$ values of 0 and 700 sec/mm$^2$ were used and (0.92 ± 0.05) × $10^{-3}$ mm$^2$/sec and (1.59 ± 0.04) × $10^{-3}$ mm$^2$/sec, respectively, for reader 1 and (0.90 ± 0.05) × $10^{-3}$ mm$^2$/sec and (1.59 ± 0.04) × $10^{-3}$ mm$^2$/sec, respectively, for reader 2 in patients in whom $b$ values of 0 and 1000 sec/mm$^2$ were used (Table 3, Fig 5). Based on a regression model that included an interaction term between tissue type (cancer lesions and healthy prostate) and subgroup ($b$ = 700 sec/mm$^2$ and $b$ = 1000 sec/mm$^2$), the difference in the ADC overlap between patients imaged at the two different $b$ values was not significant ($P = .23$). The number of lesions in the transition zone was too small for analysis.

In the 73 cancer foci that could be visualized on DW MR images, a higher Gleason score was significantly associated with both a lower mean ADC

**Table 3**

**Mean ADCs of Cancerous Regions and Healthy Prostatic Tissue in the Peripheral Zone**

| Group | No. of Lesions | Mean ADC (× $10^3$ mm$^2$/sec)* | | *P* Value |
|---|---|---|---|---|
| | | Healthy Tissue | Cancerous Lesion | |
| | | Reader 1 | | |
| All DW MR studies | 58 | 1.81 ± 0.06 | 1.09 ± 0.06 | <.001 |
| *b* value of 700 sec/mm$^2$ | 24 | 2.14 ± 0.10 | 1.33 ± 0.10 | <.001 |
| *b* value of 1000 sec/mm$^2$ | 34 | 1.59 ± 0.04 | 0.92 ± 0.05 | <.001 |
| | | Reader 2 | | |
| All DW MR studies | 55 | 1.81 ± 0.06 | 1.08 ± 0.06 | <.001 |
| *b* value of 700 sec/mm$^2$ | 23 | 2.14 ± 0.10 | 1.33 ± 0.10 | <.001 |
| *b* value of 1000 sec/mm$^2$ | 32 | 1.59 ± 0.04 | 0.90 ± 0.05 | <.001 |

* Data are means ± standard errors.

**Figure 5**

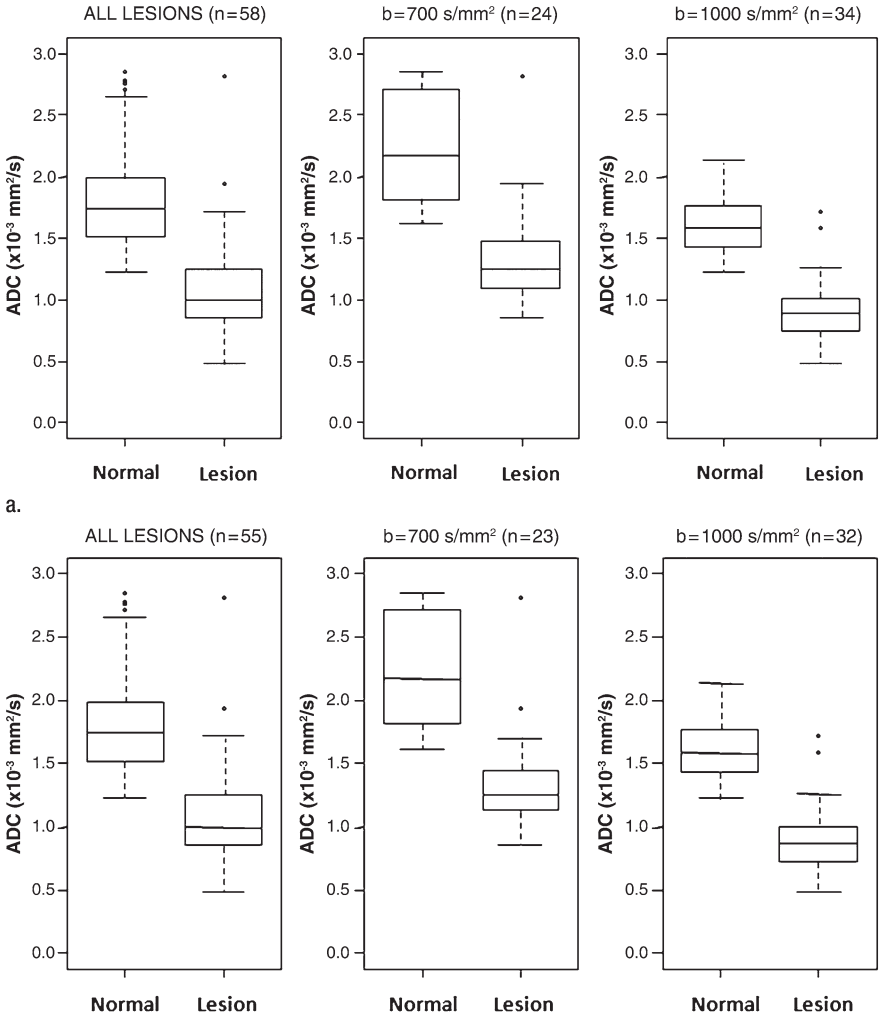


**Figure 5:** Box and whisker plots show ADCs (in $mm^2$/sec *[$mm^2$/s]*) of prostate cancer lesions *(Lesion)* and healthy prostate tissue *(Normal)* at *b* values of 700 and 1000 sec/$mm^2$ *(s/$mm^2$)* for readers **(a)** 1 and **(b)** 2. Center line = median, top of box = 75th percentile, bottom of box = 25th percentile, whiskers = 10th and 90th percentiles, ● = outlier.

($P$ = .017) and a lower mean ADC ratio ($P$ = .016) (Fig 6). The mean ADCs and mean ADC ratios of lesions with Gleason scores 6, 7, and 8 or higher differed significantly, with lower ADCs observed with increasing Gleason scores (Fig 6).

## Discussion

A number of studies, using various image acquisition methods and reference standards, have reported improved prostate cancer detection by using combined T2-weighted and DW MR imaging as compared with T2-weighted MR imaging alone (Table 4) (10,11,19–21). In our study, the accuracy of prostate cancer detection with T2-weighted MR imaging (AUC of about 0.80) was within the range reported in the prior studies (10,11,19–21). However, we did not observe clinically important incremental value with the addition of DW MR imaging (the AUC for one reader remained at 0.79, while the AUC for the other reader increased from 0.76 to 0.78). It has been suggested that the diagnostic performance of MR imaging in prostate cancer detection could be decreased when there is a preponderance of lower Gleason score tumors (22), which is relevant given the trend toward less aggressive prostate cancer reported in the United States in the recent literature (23), although this trend varies worldwide (24). In our study, readers detected only 53%–63% of Gleason 3 + 3 tumors but detected all tumors that had a Gleason score of 8 or higher, although the latter represented only 4% of the total number of tumors in our study population. Furthermore, 18% (16 of 89) of cancer foci identified at step-section pathologic analysis were not visible on DW MR images, even after retrospective unblinded review. Demographic changes may have also led to a shift in the proportion of sparse cancer foci (ie, foci of which more than 50% of the cross-sectional area is primarily healthy glandular tissue), which may affect detection on MR images, particularly in less aggressive (ie, Gleason score 3 + 3) tumors (25).

Our results indicate that the greatest added value of DW MR imaging may lie in its ability to be used to quantitatively assess prostate cancer aggressiveness. By using whole-mount step-section pathologic analysis as the standard of reference, we found a significant inverse correlation between lower ADCs and higher Gleason scores: Mean ADCs were (1.21, 1.10, 0.87 and 0.69) $\times 10^{-3}$ $mm^2$/sec for prostate cancers with Gleason scores of 3 + 3, 3 + 4, 4 + 3, and 8 or higher, respectively ($P$ = .017).

While DW MR imaging is attracting research and clinical interest as a quantitative method to assess prostate cancer aggressiveness, it is still an evolving technique that needs comprehensive investigation and standardization of its acquisition and image analysis methods. Previous studies have reported mean ADCs ranging from 0.93 $\times 10^{-3}$ $mm^2$/sec to 1.58 $\times 10^{-3}$ $mm^2$/sec for cancerous regions and from 1.61 $\times 10^{-3}$ $mm^2$/sec to 2.61 $\times 10^{-3}$ $mm^2$/sec for healthy peripheral zone tissue (10,26–33). This wide variation in ADCs is owing, at least partly, to technical factors involving the DW MR imaging sequence acquisition. ADCs are dependent on many factors, in particular the magnetic field strength;

**Table 4**

**Summary of Previous Studies of DW MR Imaging for Prostate Cancer Detection**

| Study | No. of Patients | Magnet (T) | Endorectal Coil | *b* Value or Values (sec/mm$^2$) | Performance* | | Reference Standard |
|---|---|---|---|---|---|---|---|
| | | | | | T2-weighted MR Imaging | DW MR Imaging | |
| Lim et al (19) | 52 | 1.5 | Yes | 1000 | 0.66–0.79† | 0.76–0.90† | Whole-mount |
| Haider et al (20) | 49 | 1.5 | Yes | 600 | 0.81 | 0.89 | Whole-mount |
| Miao et al (11) | 37 | 3.0 | No | 300, 600 | 0.84 | 0.89 | Biopsy |
| Kitajima et al (21) | 53 | 3.0 | No | 300, 600 | 0.82 | 0.89 | Biopsy |
| Kim et al (10)‡ | 37 | 3.0 | No | 1000 | 0.66, 0.63§ | 0.84, 0.86§ | Whole-mount |

* Unless otherwise indicated, data are AUCs.

† AUC range for three independent readers.

‡ Lesion-by-lesion analysis; therefore, specificity, negative predictive value, and accuracy could not be calculated.

§ Data are sensitivity, followed by positive predictive value.

the amplitudes, lengths, and intervals between the diffusion gradients (indicated by the *b* values); and the mathematic model used for fitting the signal decay data observed at different *b* values (34). In theory, larger *b* values are more sensitive to slower motion of water molecules and smaller diffusion distances and, therefore, provide better contrast and less T2 shine-through effect (35). The signal-to-noise ratio, however, decreases as the *b* values increase, affecting the imaging quality. The ADCs also decrease as the *b* values increase. As expected, the mean ADCs for both cancerous and noncancerous regions were lower when DW MR imaging was performed by using a *b* value of 1000 sec/mm$^2$ than when a *b* value of 700 sec/mm$^2$ was used. Owing to the lack of standardized equipment and protocols, it is not possible at this time to establish a threshold ADC to determine the presence of malignancy.

By using multiple *b* values (0, 100, 300, 500, and 800 sec/mm$^2$), deSouza et al (36) examined 44 patients at 1.5 T and fitted the DW MR imaging data at *b* values of 0–100 sec/mm$^2$ to reflect a fast diffusion component (microcapillary perfusion) and data at *b* values of 100–800 sec/mm$^2$ to reflect a slow diffusion component (intra- and extracellular water movement over a short diffusion length). They found that mean fast and slow ADCs from prostate cancer differed significantly between low-risk (biopsy Gleason score of ≤6 and prostate-specific antigen level of <10 ng/mL) and high-risk (biopsy Gleason score of ≥7 or prostate-specific antigen level of ≥10 ng/mL) groups. Another study (37) of 57 men undergoing 1.5-T DW MR imaging using *b* values of 0 and 1000 sec/mm$^2$ found significantly different mean ADCs for lesions with biopsy Gleason scores of 6, 7, and 8 (mean ADCs of [0.86, 0.70, and 0.67] × $10^{-3}$ mm$^2$/sec, respectively; $P < .05$). However, both

**Figure 6**

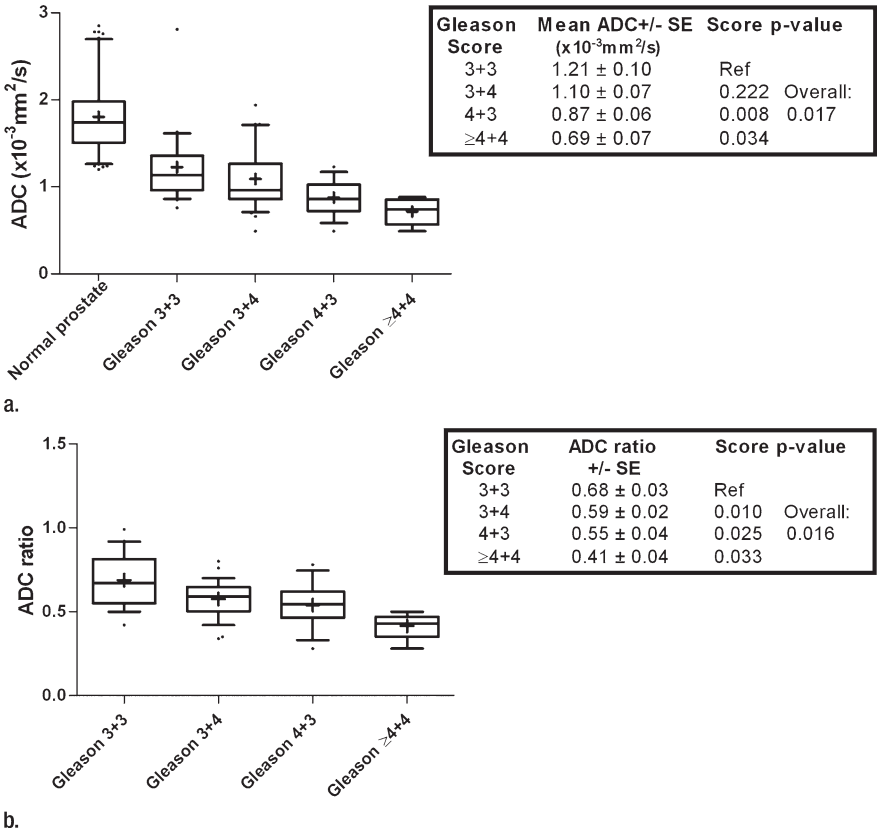


**Figure 6:** Box and whisker plots show **(a)** ADCs (in mm$^2$/sec *[mm$^2$/s]*) and **(b)** ADC ratios of lesions detected on ADC maps stratified by Gleason score. Center line = median, + = mean, top of box = 75th percentile, bottom of box = 25th percentile, whiskers = 10th and 90th percentiles, ● = outlier. *Ref* = reference value, *SE* = standard error.

of these studies (36,37) are subject to the inherent limitations of using biopsy samples as a reference standard. Final Gleason score established from the prostatectomy specimen differs from the biopsy Gleason score in 42%–69% of patients (38–40). This discrepancy, which was also found in 43% of the patients in our study, is generally attributed to sampling error during biopsies as well as the multifocal and histologically heterogeneous nature of prostate cancer (38,39). Thus, any technique being proposed for predicting aggressiveness should be evaluated, ideally, by using whole-mount prostatectomy specimens as the reference standard. Kim et al (26) found no association between tumor ADCs in 35 patients (obtained at 3 T with *b* values of 0 and 1000 sec/mm$^2$) and prostatectomy Gleason scores or prostate-specific antigen levels, but no endorectal coil was used in their study.

Our study was limited by its retrospective design and relatively small sample size. The results are based on the findings from only two independent readers with intermediate levels of experience (2 and 4 years) in prostate MR imaging. It is possible that the effect of adding DW MR imaging would be different for readers with different levels of experience, as other techniques, such as MR spectroscopy (41) and dynamic contrast-enhanced MR imaging (42), have been found to offer more significant improvements in diagnostic performance for inexperienced readers than for experienced readers. Furthermore, there is a possibility of selection bias, since only patients who underwent radical prostatectomy were included; however, this was necessary to be able to use whole-mount step-section pathologic findings as the reference standard. Our study was also limited by the use of different *b* values (700 and 1000 sec/mm$^2$), although the ideal *b* values to be used in prostate DW MR imaging have not been established. Theoretically, higher *b* values result in increased signal-to-noise ratios, but they also result in increased echo times, which in turn translate into greater distortion. We did not directly explore the influence of echo time on diagnostic accuracy, but since the ADC is not considered a function of echo time, its variability should not affect the quantitative aspect of our study. In the future, improved technology (eg, better coils and/or parallel imaging with increased acceleration factors) should allow shorter echo times, which should reduce the amount of distortion and potentially improve overall interpretation.

In summary, we believe that the added clinical value of DW MR imaging lies in its potential to assess prostate cancer aggressiveness. As quantitative ADCs correlated significantly with tumor Gleason scores, DW MR imaging may serve as an important clinical tool by adding information about prostate cancer aggressiveness to the morphologic information provided by T2-weighted MR imaging. Further studies are necessary to determine the prognostic and predictive effect of DW MR imaging in various patient populations by using clinical outcomes as the reference standard.

**Acknowledgment:** We are grateful to Ada Muellner, MS, for editing this manuscript.

**Disclosures of Potential Conflicts of Interest:** **H.A.V.** No potential conflicts of interest to disclose. **O.A.** No potential conflicts of interest to disclose. **T.F.** No potential conflicts of interest to disclose. **Y.M.** No potential conflicts of interest to disclose. **J.Z.** No potential conflicts of interest to disclose. **C.M.** No potential conflicts of interest to disclose. **K.U.** No potential conflicts of interest to disclose. **J.E.** No potential conflicts of interest to disclose. **H.H.** No potential conflicts of interest to disclose.

## References

1. Jemal A, Siegel R, Xu J, Ward E. Cancer statistics, 2010. CA Cancer J Clin 2010;60(5):277–300.
2. Akin O, Hricak H. Imaging of prostate cancer. Radiol Clin North Am 2007;45(1):207–222.
3. Fuchsjäger M, Akin O, Shukla-Dave A, Pucar D, Hricak H. The role of MRI and MRSI in diagnosis, treatment selection, and post-treatment follow-up for prostate cancer. Clin Adv Hematol Oncol 2009;7(3):193–202.
4. Turkbey B, Albert PS, Kurdziel K, Choyke PL. Imaging localized prostate cancer: current approaches and new developments. AJR Am J Roentgenol 2009;192(6):1471–1480.
5. Kurhanewicz J, Vigneron D, Carroll P, Coakley F. Multiparametric magnetic resonance imaging in prostate cancer: present and future. Curr Opin Urol 2008;18(1):71–77.
6. Engelbrecht MR, Puech P, Colin P, Akin O, Lemaître L, Villers A. Multimodality magnetic resonance imaging of prostate cancer. J Endourol 2010;24(5):677–684.
7. Kim CK, Park BK, Kim B. Diffusion-weighted MRI at 3 T for the evaluation of prostate cancer. AJR Am J Roentgenol 2010;194(6):1461–1469.
8. Gibbs P, Pickles MD, Turnbull LW. Diffusion imaging of the prostate at 3.0 tesla. Invest Radiol 2006;41(2):185–188.
9. Pickles MD, Gibbs P, Sreenivas M, Turnbull LW. Diffusion-weighted imaging of normal and malignant prostate tissue at 3.0T. J Magn Reson Imaging 2006;23(2):130–134.
10. Kim CK, Park BK, Lee HM, Kwon GY. Value of diffusion-weighted imaging for the prediction of prostate cancer location at 3T using a phased-array coil: preliminary results. Invest Radiol 2007;42(12):842–847.
11. Miao H, Fukatsu H, Ishigaki T. Prostate cancer detection with 3-T MRI: comparison of diffusion-weighted and T2-weighted imaging. Eur J Radiol 2007;61(2):297–302.
12. Zhou XH, Obuchowski NA, McClish DK. Statistical methods in diagnostic medicine. New York, NY: Wiley, 2002.
13. Leisenring W, Alonzo T, Pepe MS. Comparisons of predictive values of binary medical diagnostic tests for paired designs. Biometrics 2000;56(2):345–351.
14. Obuchowski NA. Nonparametric analysis of clustered ROC curve data. Biometrics 1997;53(2):567–578.
15. Obuchowski NA, Mazzone PJ, Dachman AH. Bias, underestimation of risk, and loss of statistical power in patient-level analyses of lesion detection. Eur Radiol 2010;20(3):584–594.
16. Cohen J. Weighted kappa: nominal scale agreement with provision for scaled disagreement or partial credit. Psychol Bull 1968;70(4):213–220.
17. Landis JR, Koch GG. The measurement of observer agreement for categorical data. Biometrics 1977;33(1):159–174.
18. Feinstein AR. Invidious comparisons and unmet clinical challenges. Am J Med 1992;92(2):117–120.
19. Lim HK, Kim JK, Kim KA, Cho KS. Prostate cancer: apparent diffusion coefficient map with T2-weighted images for detection—a multireader study. Radiology 2009;250(1):145–151.
20. Haider MA, van der Kwast TH, Tanguay J, et al. Combined T2-weighted and diffusion-weighted MRI for localization of prostate cancer. AJR Am J Roentgenol 2007;189(2):323–328.

21. Kitajima K, Kaji Y, Fukabori Y, Yoshida K, Suganuma N, Sugimura K. Prostate cancer detection with 3 T MRI: comparison of diffusion-weighted imaging and dynamic contrast-enhanced MRI in combination with T2-weighted imaging. J Magn Reson Imaging 2010;31(3):625–631.

22. Hricak H, Choyke PL, Eberhardt SC, Leibel SA, Scardino PT. Imaging prostate cancer: a multidisciplinary perspective. Radiology 2007; 243(1):28–53.

23. Surveillance, Epidemiology and End Results (SEER) program. SEER 17 registries, 2004-2006. In: Division of cancer control and population science. Bethesda, Md: National Cancer Institute, 2009.

24. Sloan FA, Gelband H, eds; Committee on Cancer Control in Low- and Middle-Income Countries, Board on Global Health, Institute of Medicine of the National Academies. Cancer control opportunities in low- and middle-income countries. Washington, DC: National Academies Press, 2007.

25. Langer DL, van der Kwast TH, Evans AJ, et al. Intermixed normal tissue within prostate cancer: effect on MR imaging measurements of apparent diffusion coefficient and T2—sparse versus dense cancers. Radiology 2008;249(3):900–908.

26. Kim CK, Park BK, Han JJ, Kang TW, Lee HM. Diffusion-weighted imaging of the prostate at 3 T for differentiation of malignant and benign tissue in transition and peripheral zones: preliminary results. J Comput Assist Tomogr 2007;31(3):449–454.

27. Gibbs P, Liney GP, Pickles MD, Zelhof B, Rodrigues G, Turnbull LW. Correlation of ADC and T2 measurements with cell density in prostate cancer at 3.0 Tesla. Invest Radiol 2009;44(9):572–576.

28. Tamada T, Sone T, Jo Y, et al. Apparent diffusion coefficient values in peripheral and transition zones of the prostate: comparison between normal and malignant prostatic tissues and correlation with histologic grade. J Magn Reson Imaging 2008;28(3): 720–726.

29. Issa B. In vivo measurement of the apparent diffusion coefficient in normal and malignant prostatic tissues using echo-planar imaging. J Magn Reson Imaging 2002;16(2): 196–200.

30. Chan I, Wells W 3rd, Mulkern RV, et al. Detection of prostate cancer by integration of line-scan diffusion, T2-mapping and T2-weighted magnetic resonance imaging; a multichannel statistical classifier. Med Phys 2003;30(9):2390–2398.

31. Hosseinzadeh K, Schwarz SD. Endorectal diffusion-weighted imaging in prostate cancer to differentiate malignant and benign peripheral zone tissue. J Magn Reson Imaging 2004;20(4):654–661.

32. Tanimoto A, Nakashima J, Kohno H, Shinmoto H, Kuribayashi S. Prostate cancer screening: the clinical value of diffusion-weighted imaging and dynamic MR imaging in combination with T2-weighted imaging. J Magn Reson Imaging 2007;25(1):146–152.

33. Sato C, Naganawa S, Nakamura T, et al. Differentiation of noncancerous tissue and cancer lesions by apparent diffusion coefficient values in transition and peripheral zones of the prostate. J Magn Reson Imaging 2005;21(3):258–262.

34. Riches SF, Hawtin K, Charles-Edwards EM, de Souza NM. Diffusion-weighted imaging of the prostate and rectal wall: comparison of biexponential and monoexponential modelled diffusion and associated perfusion coefficients. NMR Biomed 2009;22(3): 318–325.

35. DeLano MC, Cooper TG, Siebert JE, Potchen MJ, Kuppusamy K. High-b-value diffusion-weighted MR imaging of adult brain: image contrast and apparent diffusion coefficient map features. AJNR Am J Neuroradiol 2000; 21(10):1830–1836.

36. deSouza NM, Riches SF, Vanas NJ, et al. Diffusion-weighted magnetic resonance imaging: a potential non-invasive marker of tumour aggressiveness in localized prostate cancer. Clin Radiol 2008;63(7):774–782.

37. Woodfield CA, Tung GA, Grand DJ, Pezzullo JA, Machan JT, Renzulli JF 2nd. Diffusion-weighted MRI of peripheral zone prostate cancer: comparison of tumor apparent diffusion coefficient with Gleason score and percentage of tumor on core biopsy. AJR Am J Roentgenol 2010;194(4):W316–W322.

38. Cookson MS, Fleshner NE, Soloway SM, Fair WR. Correlation between Gleason score of needle biopsy and radical prostatectomy specimen: accuracy and clinical implications. J Urol 1997;157(2):559–562.

39. Steinberg DM, Sauvageot J, Piantadosi S, Epstein JI. Correlation of prostate needle biopsy and radical prostatectomy Gleason grade in academic and community settings. Am J Surg Pathol 1997;21(5):566–576.

40. Zakian KL, Sircar K, Hricak H, et al. Correlation of proton MR spectroscopic imaging with Gleason score based on step-section pathologic analysis after radical prostatectomy. Radiology 2005;234(3):804–814.

41. Yu KK, Scheidler J, Hricak H, et al. Prostate cancer: prediction of extracapsular extension with endorectal MR imaging and three-dimensional proton MR spectroscopic imaging. Radiology 1999;213(2):481–488.

42. Fütterer JJ, Engelbrecht MR, Huisman HJ, et al. Staging prostate cancer with dynamic contrast-enhanced endorectal MR imaging prior to radical prostatectomy: experienced versus less experienced readers. Radiology 2005;237(2):541–549.